

1 **When does vapor pressure deficit drive or reduce**
2 **evapotranspiration?**

3 **A. Massmann¹, P. Gentine¹, C. Lin²**

4 ¹Department of Earth and Environmental Engineering, Columbia University, New York, NY 10027

5 ²Department of Hydraulic Engineering, Tsinghua University, Beijing, CN

6 **Key Points:**

- 7 • = enter point 1 here =
8 • = enter point 2 here =
9 • = enter point 3 here =

10 **Abstract**

11 = enter abstract here =

12 **1 Introduction**

13 Changes to vapor pressure deficit (VPD) alter the atmospheric demand for water from
 14 the land surface. Traditionally, atmospheric scientists and hydrometeorologists generally
 15 think that an increase in atmospheric demand induces an increases in evapotranspiration
 16 (ET) (citations?). This possible misconception developed in part due to the proliferation of
 17 studies examining potential ET (PET) rather than estimates of ET itself (citations?). In con-
 18 trast, plant physiologists know that stomata have evolved to optimally regulate the exchange
 19 of water and carbon, and tend to close in response to increased atmospheric dryness [Ball
 20 *et al.*, 1987; Leuning, 1990; MEDLYN *et al.*, 2011]. Therefore, an increase (decrease) in
 21 VPD may not correspond to an increase (decrease) in ET because stomatal closure (opening)
 22 can cancel the effects of shifts to atmospheric demand.

← This section
needs to be
fleshed out,
and I defi-
nitely need
to add more
citations

23 Quantifying the plant response to a perturbation to atmospheric VPD increases our un-
 24 derstanding of land surface response to shifts in atmospheric conditions. If plant response
 25 reduces ET in response to atmospheric drying then soil moisture will be conserved. An in-
 26 crease in ET in response to atmospheric drying will reduce soil moisture, but contribute in-
 27 creased moistening to the atmosphere. Clearly, the sign and magnitude of land-surface
 28 response drives the co-evolution of the atmosphere and land-surface at many timescales, from
 29 diurnal to interdecadal.

30 We hypothesize that for most plant types a common response to increase in VPD will
 31 actually be a decrease in ET. The exception would be plants such as crops that are evolved (or
 32 bred) to prioritize gross primary production (GPP) over water conservation. However, for all
 33 other plant types, our hypothesis calls into question the validity of PET-based drought met-
 34 rics developed by hydrometeorologists and used extensively in operations [e.g. PDSI, P-PET,
 35 200, 2002; Alley, 1984]. These metrics ignore the role of plants as gatekeepers for surface
 36 water loss to the atmosphere and have limited physical meaning for drought of vegetated land
 37 types. Additionally, plants evolved in arid climates should prioritize water conservation and
 38 we would expect a very negative ET response to increase in VPD. Therefore, vegetated loca-
 39 tions most likely to experience droughts should show the strongest deviation between reality
 40 and a PET-based approximation.

← more cita-
tions needed,
including
recent PET
climate stud-
ies like Jack
Scheff

41 In order to quantify plant response to perturbations to atmospheric demand for water,
 42 we apply a Penman-Monteith framework to eddy-covariance observation spanning various
 43 biomes and climates. Section 2 describes the data used, Section 3 derives the framework,
 44 Section 4 presents results, and Section 5 discusses conclusions. The goal of this paper is
 45 to use reasonable approximations as a tool to increase intuition for plant response to atmo-
 46 spheric drying. This intuition will aid interpretation of observations and full complexity cli-
 47 mate models.

48 **2 Methods**

49 The Penman-Monteith equation (hereafter PM) estimates ET as a function of atmo-
 50 spheric and land-surface variables:

$$51 \quad ET = \frac{\Delta R + g_a \rho_a c_p D_s}{\Delta + \gamma(1 + \frac{g_a}{g_s})}, \quad (1)$$

52 where variable definitions are given in Table 1. *MEDLYN et al.* [2011] developed a
 53 model for g_s by combining optimal photosynthesis theory with empirical approaches. The
 54 result for leaf-scale stomatal resistance was:

$$55 \quad g_{l-s} = g_0 + 1.6 \left(1 + \frac{g_1}{\sqrt{D_s}} \right) \frac{A}{c_s} \quad (2)$$

56 This can be adapted to an ecosystem-scale stomatal resistance by multiplying by leaf
 57 area index (LAI) and converting units to m s^{-1}

$$58 \quad g_s = \text{LAI} \frac{R T}{P} \left(g_0 + 1.6 \left(1 + \frac{g_1}{\sqrt{D_s}} \right) \frac{A}{c_s} \right) \quad (3)$$

59 While Equation 3 can be used in PM, it will make analytical work with the function
 60 intractable because A is a function of ET itself. To remove dependence of ET on A we can
 61 use the semi-empirical results of *Zhou et al.* [2015]. *Zhou et al.* [2015] showed that:

$$62 \quad uWUE = \frac{GPP \cdot \sqrt{D}}{ET} \quad (4)$$

63 is relatively constant across time and space (within plant functional type). If, following *Lin*
 64 *et al.* [2015], we approximate g_0 as 0, we can use uWUE to remove A from g_s in a way that
 65 makes PM analytically tractable:

$$g_s = \frac{RT}{P} 1.6 \left(1 + \frac{g_1}{\sqrt{D_s}}\right) \frac{\sigma \text{ uWUE } ET}{c_s \sqrt{D}} \quad (5)$$

Note that uWUE is fit on the ecosystem scale in *Zhou et al.* [2015] so GPP in 4 is really $A \cdot \text{LAI}$. This leads to the cancelation of LAI in additoin to uWUE in Equation 2. We also recognize that our use of uWUE introudces considerable uncertainty, so we added an uncertainty parameter $\sigma = f(t, \text{site})$ modifying uWUE . The meaning of this parameter will be elaborated on after the derivation of $\frac{\partial ET}{\partial D}$.

Next, plugging Equation 5 into Equation 1 and rearranging gives:

$$ET = \frac{\Delta R + \frac{g_a P}{T} \left(\frac{c_p D_s}{R_{air}} - \frac{\gamma c_s \sqrt{D}}{R * 1.6 \sigma \text{ uWUE} (1 + \frac{g_1}{\sqrt{D}})} \right)}{\Delta + \gamma} \quad (6)$$

Note that if we set the uncertaitny parameter σ to 1, and approximage c_s at a global mean CO₂ concentration, then Equation 6 is fully defined using commonly available weather station data and the constants published in *Zhou et al.* [2015]; *Lin et al.* [2015]. This then begs the question, why use PET at all for drought metrics in vegetated areas? A much more physically realistic estimate of ET can be had with the same information requiured to calculate PET.

We can now take the derivative with respect to D to analytically determine ecosystem response to atmospheric demand perturbations:

$$\frac{\partial ET}{\partial D} = \frac{g_a P}{T(\Delta + \gamma)} \left(\frac{c_p}{R_{air}} - \frac{\gamma c_s}{1.6 R * \sigma \text{ uWUE}} \left(\frac{2g_1 + \sqrt{D}}{2(g_1 + \sqrt{D})^2} \right) \right) \quad (7)$$

The D dependence in Equation 7 is a little opaque. However, mean D is 1062 Pa, so \sqrt{D} is 32.6 Pa^{1/2}, which is much less than g_1 (with the exception of ENF; Table 3). So a series expansion in the limit $\frac{\sqrt{D}}{g_1} \rightarrow 0$ gives an approximation which makes the functional form more clear:

$$\frac{\partial ET}{\partial D} \approx \frac{g_a P}{T(\Delta + \gamma)} \left(\frac{c_p}{R_{air}} - \frac{\gamma c_s}{1.6 R * \sigma \text{ uWUE}} \left(\frac{1}{g_1} - \frac{3\sqrt{D}}{2g_1^2} + \frac{2\sqrt{D}^2}{g_1^3} - \frac{5\sqrt{D}^3}{2g_1^4} + O\left(\left(\frac{\sqrt{D}}{g_1}\right)^4\right) \right) \right) \quad (8)$$

Note that given yearly uWUE from *Zhou et al.* [2015], g_1 from *Lin et al.* [2015] [as presented in *Franks et al.*, 2017], and observations of R , T , P , D_s , and wind speed (WS), all

99

Table 1. Definition of symbols and variables

Variable	Description	Units
e_s	saturation vapor pressure	Pa
T	temperature	K
Δ	$\frac{\partial e_s}{\partial T}$	Pa K ⁻¹
R	net radiation at land surface minus ground heat flux	W m ⁻²
g_a	aerodynamic conductance	m s ⁻¹
ρ_a	air density	kg m ⁻³
c_p	specific heat capacity of air at constant pressure	J K ⁻¹ kg ⁻¹
D	VPD	Pa
γ	psychrometric constant	Pa K ⁻¹
g_s	stomatal conductance	m s ⁻¹
g_{l-s}	leaf-scale stomatal conductance	mol m ⁻² s ⁻¹
R^*	universal gas constant	J mol ⁻¹ K ⁻¹
LAI	leaf area index	-
σ	uncertainty parameter	-
c_s	CO ₂ concentration	μ mol CO ₂ mol ⁻¹ air

^aFootnote text here.

90

quantities in Equations 7 and 8 are known except for the uncertainty parameter σ . With flux tower observations of ET, σ will then be uniquely determined for each observation through Equation 6:

93

$$\sigma = - \frac{g_a \gamma c_s \sqrt{D_s} P}{(ET(\Delta + \gamma) - \Delta R - g_a \rho_a c_p D_s) 1.6 R T uWUE (1 + \frac{g_s}{\sqrt{D_s}})} \quad (9)$$

94

This σ will be some part uncertainty associated with assumptions about constant g_1 and $uWUE$, including differences between the data used here and in the fits in Zhou *et al.* [2015] and Lin *et al.* [2015], but also some part general PM model and FLUXNET observational uncertainty. By calculating a unique σ for each observation we will propagate any model and observational uncertainty forward into our expression for $\frac{\partial ET}{\partial D}$.

104 **Table 2.** Plant functional types, their abbreviation, Medlyn coefficient [from *Lin et al.*, 2015], and uWfUE
 105 [from *Zhou et al.*, 2015]. Note that units are converted such that the quantities fit into Equations 1-8 with the
 106 variables in Table 1.

Abbreviation	PFT	g_1 ($\text{Pa}^{0.5}$)	uWUE ($\mu\text{-mol [C]} \text{ Pa}^{0.5} \text{ J}^{-1} [\text{ET}]$)
CRO	cropland	183.1	3.80
CSH	closed shrub	148.6	2.18
DBF	deciduous broadleaf forest	140.7	3.12
ENF	evergreen needleleaf forest	74.3	3.30
GRA	grassland (C3)	166.0	2.68

“Footnote text here.

100 3 Data

101 We use data from FLUXNET2015. Because g_1 coefficients [*Lin et al.*, 2015] and uWUE
 102 were only both available for five plant functional types (PFTs - see Table 3), only 56 of the 77
 103 sites were used. Figure 1 presents each site and its plant functional type.

← map needs
to be im-
proved - it's
a placeholder
for now

104 We restrict our analysis to the daytime (sensible heat $> 5 \text{ W m}^{-2}$ and shortwave radia-
 105 tion $> 50 \text{ W m}^{-2}$) when there is no precipitation and the plants are growing (GPP $> 10\%$ of
 106 the 95th percentile). Also, because some sites use half hourly data but some use hourly, we
 107 aggregate all data to hourly averages. Only times with good quality control flags are used.

← This GPP
thresholding
was used by
Changjie, do
you know if
there is a ci-
tation for it?
Otherwise it
seems like
something
a reviewer
would have
issue with as
it is arbitray

113 4 Results

114 By construction, the variability in the σ term (Equation 9) contains all model and ob-
 115 servational uncertainties. For an observation that perfectly matches our model and assump-
 116 tions σ will be one. Therefore, if for our assumptions and framework to be reasonable σ
 117 should be $O(1)$. Figure 2 presents the histogram of calculated σ s with outliers (lowest and
 118 highest 5% percent) and nonphysical values ($\sigma < 0$) removed. All remaining σ values are
 119 $O(1)$ which provides confidence in model framework.

123 An additional concern is that the σ term may in fact be some function of D , in which
 124 case the dependence would need to be accounted for when taking the derivative. Figure 3
 125 plots the joint distribution of σ and VPD, and shows that σ is very weakly a function of

← Figs 2 and 3
can probably
be combined
- the his-
togram of σ
is shown in
Fig 3.

126 VPD. Given this weak dependence, we argue that Equation 7 is a valid approximation for
 127 ET response to D .

132 Before calculating the sensitivity of ET to VPD, it is useful to consider the functional
 133 form of Equation 7. There are three terms: a scaling term for the full expression we will call
 134 Term 1 ($\frac{g_a P}{T(\Delta+\gamma)}$), a relatively constant offset we will call Term 2 ($\frac{c_p}{R_{air}}$), and a variable term
 135 we will call Term 3 ($\frac{\gamma c_s}{1.6 R \text{ uWUE}} \left(\frac{2g_1 + \sqrt{D}}{2(g_1 + \sqrt{D})^2} \right)$). All variables are positive, so the relative mag-
 136 nitude between Term 2 and Term 3 will determine the sign of the derivative, while Term 1
 137 will scale the expression larger or smaller.

138 In Term 1, $\frac{P}{T} \propto \rho$, so this should vary little relative to aerodynamic conductance and
 139 Δ . γ should also be relatively constant, so the scaling term, Term 1, should be primarily a
 140 function of aerodynamic conductance and temperature (through the function Δ). This makes
 141 sense, as aerodynamic conductance represents how efficiently response at the surface is com-
 142 municated to the atmosphere. As it increases, any plant response will be communicated more
 143 strongly to the atmosphere (and vice-versa).

144 Δ 's presence in the scaling term also matches physical intuition. Evaporative cooling
 145 will dampen the ability of the atmosphere to take more moisture, as e_{sat} decreases with
 146 temperature.. The decrease in e_{sat} is proportional to $\Delta (\delta e_{sat} = \Delta \delta T)$. So as Δ increases,
 147 you will get a larger damping of ET due to evaporative cooling. The functional form of Δ
 148 will be the same across PFT, but the temperature range may vary slightly. In contrast, aero-
 149 dynamic conductance will vary strongly with PFT due to the importance of surface rough-
 150 ness. So most of the differences in scaling between PFT should be in the aerodynamic con-
 151 ductance term. One interesting side note is that the coefficient of variability for both aero-
 152 dynamic conductance and Term 1 is relatively constant across PFT, suggesting that the influ-
 153 ence of aerodynamic conductance on the relative (to the PFT mean) variability of Term 1 is
 154 approximately similar across PFT.

155 Figure 4A shows Term 1 normalized by mean aerodynamic conductance (calculated
 156 for each plant functional type), and confirms that much of the relative variability of Term 1
 157 is contained in the aerodynamic conductance variability. Generally, T has less of a role. Ad-
 158 ditionally, the impact of T on the relative variability increases with increasing aerodynamic
 159 conductance. .

← plot every
PFT and
show they
collapse onto
the same
curve? -
might just be
too messy
though

160 While the relative variability of Term 1 is similar across PFT, the absolute value of
 161 Term 1 varies strongly across PFT. Figure 4B shows Term 1 evaluated with the mean aerody-
 162 namic conductance for each PFT, and at the range of observed temperatures for each PFT. As
 163 expected, for the tree PFTs (DBF, ENF) Term 1 is much larger and the temperature depen-
 164 dence is much stronger. Systematic differences in observed temperatures also cause differ-
 165 ences in the average magnitude of Term 1. For example, ENF experiences on average colder
 166 temperatures and is thus more likely to have a larger scaling term. Additionally, because the
 167 variability of aerodynamic conductance increases proportionally to the mean, the spread of
 168 Term 1 due to aerodynamic conductance variability will be larger for the tree PFTs, although
 169 this is not shown for simplicity. To summarize, the variability of Term 1 within each PFT
 170 will look like Figure 4A for each PFT, but the scale of the y-axis will increase or decrease
 171 according to mean aerodynamic conductance oberved in Figure 4B.

176 Term 2 minus Term 3 determines the sign of the sensitivty of ET to VPD and is thus
 177 crucial. c_s variability is relatively less than σ and D variability, so variability within PFT
 178 will be solely determined by σ and D at the different fluxnet sites. Figure 5 shows how (Term
 179 2 - Term 3) varies with D and σ , as a function of PFT. Equation 8 aids interpretation of Fig-
 180 ure 5. Larger $uWUE$, $\bar{\sigma}$, and $g1$ shift the leading-order constant term ($\frac{1}{g1}$) towards smaller
 181 values, and (Term 2 - Term 3) towards positive values. $uWUE$ and $g1$ are both water-use
 182 effiency type constants. Higher values corresponde to plants that are more willing to spend
 183 water on primary production and less evolved to conserve water. Figure 5 confirms our phys-
 184 ical intuition: CROs are the least water conservative so have the smallest constant portion of
 185 Term 3, while CSH are the most water conservative and have the largest constant portion of
 186 Term 3. For the VPD-dependent terms in Equation 8, differences in $g1$ between PFTs exert a
 187 greater influence than difference $uWUE$, as the power of $g1$ increases. Increasing $uWUE$
 188 and $g1$ decreases the VPD-dependence, but $g1$ has the bigger effect due to its increasing
 189 powers. ENF ($g1 = 74.31$) has by far the largest VPD dependence of response, while CRO
 190 ($g1 = 183.1$) has the smallest VPD dependence.

197 Figure 5b shows the location of the minima of ET, as a function of σ and D . For any σ
 198 or VPD less (more) than these curves, Term 2 - Term 3 will be negative (positive). It is clear
 199 that the portion of VPD observations below/above these curves will be a strong function of
 200 σ . However, we can see some general trends. For CSH, $\frac{\partial ET}{\partial D}$ should be negative for the vast
 201 majority of observed σ and VPD. The fracion of positive $\frac{\partial ET}{\partial D}$ appears to be more even for
 202 ENF, GRA, and DBF, and we might expect a greater frequency of positive $\frac{\partial ET}{\partial D}$ for CRO.

Table 3 confirms these expectations for PFT behavior of $\frac{\partial ET}{\partial D}$. For all PFTs except for CRO, average $\frac{\partial ET}{\partial D}$ is less than zero. However, $\frac{\partial ET}{\partial D}$ evaluated at the average of all variables (e.g. σ , T , c_s , D) is only negative for CSH and GRA. And, DBF in addition to CRO experiences $\frac{\partial ET}{\partial D} < 0$ less than half the time. These observations highlight the effect of the nonlinear function in Figure 5: $\frac{\partial ET}{\partial D}$ has a much steeper slope when the function is negative, and is thus more likely to be large.

The units of $\frac{\partial ET}{\partial D}$ make it difficult to interpret if D is even a meaningful contributor to ET's variability. To better understand D 's contribution, we normalize $\frac{\partial ET}{\partial D}$ with D 's standard deviation to define a (linearized) relative change in ET for variations in D . D 's contribution to ET's variability ranges between 16 - 20 W m⁻² for all PFTs except for CSH, which is about 51 W m⁻². Another meaningful comparison is to $\frac{\partial ET}{\partial R} * std(R)$, as net radiation is generally the driver of ET (cite joe berry here). For all PFTs except for CSH D contributes between 14.5 - 20.5 % of R 's contribution to variability. For CSH the portion is much larger, about 44 %. D 's variability is certainly a non-negligible contributor to ET 's variability.

So far, idealized plots and statistics have illuminated the form of $\frac{\partial ET}{\partial D}$ and how it varies with PFT. Large mean σ and uWUE shifts CRO and DBF towards positive $\frac{\partial ET}{\partial D}$. However, the strongly nonlinear function of $\frac{\partial ET}{\partial D}$ at $\frac{\partial ET}{\partial D} < 0$ pushes $\frac{\partial ET}{\partial D}$ negative for DBF (it does not do this for CRO because of CRO's high $g1$). ENF's low $g1$ value increases the dependence of $\frac{\partial ET}{\partial D}$ on D , and makes the function more strongly nonlinear. This has the side effect of pushing $\frac{\partial ET}{\partial D}$ negative further than other PFTs for a given fraction $\frac{\partial ET}{\partial D} < 0$ and magnitude $\frac{\partial ET}{\partial D}(T, \dots, D)$. GRA shows the opposite behavior; a relatively high $g1$ makes the function more linear, decreasing the magnitude of $-\frac{\partial ET}{\partial D}$ for a given [large] fraction $\frac{\partial ET}{\partial D} < 0$ and negative $\frac{\partial ET}{\partial D}(T, \dots, D)$ (although aerodynamic conductance and Term 1 also probably have a role in this). Finally, low uWUE of CSH pushes toward by far the lowest values $\frac{\partial ET}{\partial D}$ (Figure 5). Variability in D accounts for the largest about of ET variability for CSH. For the other PFTs, D contributes less to ET variability, but still represents about 15-20 % of R 's contributions to ET variability.

4.1 Full observations of $\frac{\partial ET}{\partial D}$

Now that we have an intuitive understanding of $\frac{\partial ET}{\partial D}$'s behavior, we are equipped to interpret fully realistic plots of $\frac{\partial ET}{\partial D}$ for each PFT. Figure 6 presents calculated $\frac{\partial ET}{\partial D}$ where,

230

Table 3. Statistics of $\frac{\partial ET}{\partial D}$ as a function of PFT.

PFT	$\frac{\partial ET}{\partial VPD}$	$\frac{\partial ET}{\partial D} (\bar{T}, \dots, \bar{D})$	$\frac{\partial ET}{\partial D} (\bar{T}, \dots, \bar{D}) * \text{std}(D)$	$\frac{\frac{\partial ET}{\partial D} (\bar{T}, \dots, \bar{D}) * \text{std}(D)}{\frac{\partial ET}{\partial R} (\bar{T}, \dots, \bar{D}) * \text{std}(R)}$	fraction $\frac{\partial ET}{\partial VPD} < 0$
CRO	0.000853	0.026241	18.523659	0.203022	0.473311
CSH	-0.108234	-0.091526	50.861613	0.439379	0.931660
DBF	-0.012727	0.013794	19.734435	0.164241	0.461674
ENF	-0.034087	0.000706	16.611852	0.148548	0.534425
GRA	-0.019637	-0.000921	16.798083	0.173552	0.631735

^aFootnote text here.

234

unless otherwise noted, all variables in Equation 7 are allowed to vary. Each column is a

235

different quantity related to $\frac{\partial ET}{\partial D}$, and each row is a different PFT.

236

The full observations generally confirm expectations from Section 4. CRO has the most positive values of $\frac{\partial ET}{\partial D}$, $\frac{\partial ET}{\partial D}$ is almost always negative for CSH, and response depends more with the environmental conditions for the other PFTs (especially ENF). Through the columns of Figure 6 we can see the impact of σ and g_a on the variability of $\frac{\partial ET}{\partial D}$. g_a 's scaling (included in columns 1 and 3) alters the magnitude considerably. σ variability (included in columns 1 and 2) adds a lot of additional noise to the signal of $\frac{\partial ET}{\partial D}$, which is slightly undesirable given σ 's role in representing model and observational uncertainty. However, the general story with the noise appears to match the cleaner signal when σ is held constant and D_{ETmin} is clearly visible. One exception is possibly with GRA, for which uncertainty represented in σ is high and causes the full complexity plots (Columns 1 and 2) to not match well with σ held fixed (Columns 3 and 4).

247

For ENF and GRA D_{ETmin} does not appear to be only a function of σ (most observable in Column 4). It turns out that the site to site variability in γ causes D_{ETmin} to vary, which is not discussed in the previous section. The impact is observable in both ENF and GRA, but especially for ENF which has a larger $\frac{\partial^2 ET}{\partial^2 D}$ than the other PFTs.

← I really need
to make
these plots
better - way
too much
overlapping
of points
that hurts the
story

256

In general the full complexity plots of $\frac{\partial ET}{\partial D}$ match our expectations, even with the large sensitivity to σ measures of uncertainty observed in Figure 5. Our σ -based method of uncertainty propagation blurs the idealized expectations the most for GRA, and also has a considerable effect for CRO. We therefore have the most confidence in our conclusion based on

260 Equation 7 for PFTS CSH, DBF, and ENF, as the full complexity plots with uncertainty in-
 261 cluded closely match the story when σ is held fixed. **see somewhat preferred alternate
 262 figure 7 .

← I think I like the alternate plot much more as thinking in terms of T and RH is easier, and it makes the story easier to see at relatively low temperatures. However, I used the other plot because Fig 5 does not discuss things in terms of temperature, as this would make things more complicated (adding another dimension). I could just include both versions of figure 6 though (using figure 6a as a bridge to figure 6b)

266 5 Conclusions

267 The idealized representation of ET used here is successful in developing intuition for
 268 how ET responds to changes in D . This intuition will aid the community in interpreting ob-
 269 servations and output from sophisticated full complexity climate models.

270 The idealized framework leads to the following general conclusions:

- 271 • Aerodynamic resistance plays an important role of scaling $\frac{\partial ET}{\partial D}$. This is a leading
 272 order effect for observing higher magnitude responses in DBF and ENF.
- 273 • In general, CSH has the most negative (i.e. ET reduced) response to increases in D
 274 (atmospheric drying). So CSH plants will almost always try and conserve water, ef-
 275 fectively reducing ET with dry atmospheric perturbation.
- 276 • Additionally for CSH, D variability contributes the most to ET variability.
- 277 • CRO has the most positive response (i.e. ET increased) in response to increases in
 278 D . This is consistent with CROs that may be evolved or bred to thrive in non-water-
 279 limited environments.
- 280 • The response is more a function of the environment for DBF, ENF, and GRA. Be-
 281 cause as VPD increases the response is more likely to be positive, if RH is fixed then
 282 the response will be more likely to be positive at warmer T, or if T is fixed the re-
 283 sponse is more likely to be positive with decreasing RH.
- 284 • ENF has the strongest dependence on environmental conditions due to its small g_1 .
- 285 • Model and observational uncertainty is highest for GRA and CRO, so conclusions
 286 about those PFTs should be tempered.
- 287 • However, inclusion of uncertainty doesn't alter conclusions about DBF, ENF, and
 288 CSH.

289 The intuition developed using this framework can be used to understand how the land
 290 surface will respond and contribute to changes in the environment. Additionally, Equation 6
 291 gives provides an estimate of ET that requires no additional information beyond that required
 292 to calculate PET. Given that for all PFTs, with the exception of CRO, we found a high fre-

← also need to flesh this section out

293 quency and magnitude of negative $\frac{\partial ET}{\partial D}$, PET is a physically unrealisitic representation of
 294 ET for vegetated surfaces and PET-based drought metrics are not usefull. We advocate for
 295 drought metrics using Equation 6 instead of PET.

296 **Acknowledgments**

297 This work used eddy covariance data acquired and shared by the FLUXNET community, in-
 298 cluding these networks: AmeriFlux, AfriFlux, AsiaFlux, CarboAfrica, CarboEuropeIP, Car-
 299 boItaly, CarboMont, ChinaFlux, Fluxnet-Canada, GreenGrass, ICOS, KoFlux, LBA, NECC,
 300 OzFlux-TERN, TCOS-Siberia, and USCCC. The ERA-Interim reanalysis data are provided
 301 by ECMWF and processed by LSCE. The FLUXNET eddy covariance data processing and
 302 harmonization was carried out by the European Fluxes Database Cluster, AmeriFlux Man-
 303 agement Project, and Fluxdata project of FLUXNET, with the support of CDIAC and ICOS
 304 Ecosystem Thematic Center, and the OzFlux, ChinaFlux and AsiaFlux offices.

305 **References**

- 306 (2002), A review of twentieth-century drought indices used in the united states, *Bul-*
 307 *letin of the American Meteorological Society*, 83(8), 1149–1165, doi:10.1175/1520-
 308 0477(2002)083<1149:arotdi>2.3.co;2.
- 309 Alley, W. M. (1984), The palmer drought severity index: Limitations and assumptions,
 310 *Journal of Climate and Applied Meteorology*, 23(7), 1100–1109, doi:10.1175/1520-
 311 0450(1984)023<1100:tpdsil>2.0.co;2.
- 312 Ball, J. T., I. E. Woodrow, and J. A. Berry (1987), A model predicting stomatal conductance
 313 and its contribution to the control of photosynthesis under different environmental con-
 314 ditions, in *Progress in Photosynthesis Research*, pp. 221–224, Springer Netherlands, doi:
 315 10.1007/978-94-017-0519-6_48.
- 316 Franks, P. J., J. A. Berry, D. L. Lombardozzi, and G. B. Bonan (2017), Stomatal function
 317 across temporal and spatial scales: Deep-time trends, land-atmosphere coupling and
 318 global models, *Plant Physiology*, 174(2), 583–602, doi:10.1104/pp.17.00287.
- 319 Leuning, R. (1990), Modelling stomatal behaviour and and photosynthesis ofEucalyptus
 320 grandis, *Australian Journal of Plant Physiology*, 17(2), 159, doi:10.1071/pp9900159.
- 321 Lin, Y.-S., B. E. Medlyn, R. A. Duursma, I. C. Prentice, H. Wang, S. Baig, D. Eamus, V. R.
 322 de Dios, P. Mitchell, D. S. Ellsworth, M. O. de Beeck, G. Wallin, J. Uddling, L. Tarvainen,
 323 M.-L. Linderson, L. A. Cernusak, J. B. Nippert, T. W. Ocheltree, D. T. Tissue, N. K.

Martin-StPaul, A. Rogers, J. M. Warren, P. D. Angelis, K. Hikosaka, Q. Han, Y. Onoda, T. E. Gimeno, C. V. M. Barton, J. Bennie, D. Bonal, A. Bosc, M. LĂĽw, C. Macinins-Ng, A. Rey, L. Rowland, S. A. Setterfield, S. Tausz-Posch, J. Zaragoza-Castells, M. S. J. Broadmeadow, J. E. Drake, M. Freeman, O. Ghannoum, L. B. Hutley, J. W. Kelly, K. Kikuzawa, P. Kolari, K. Koyama, J.-M. Limousin, P. Meir, A. C. L. da Costa, T. N. Mikkelsen, N. Salinas, W. Sun, and L. Wingate (2015), Optimal stomatal behaviour around the world, *Nature Climate Change*, 5(5), 459–464, doi:10.1038/nclimate2550.

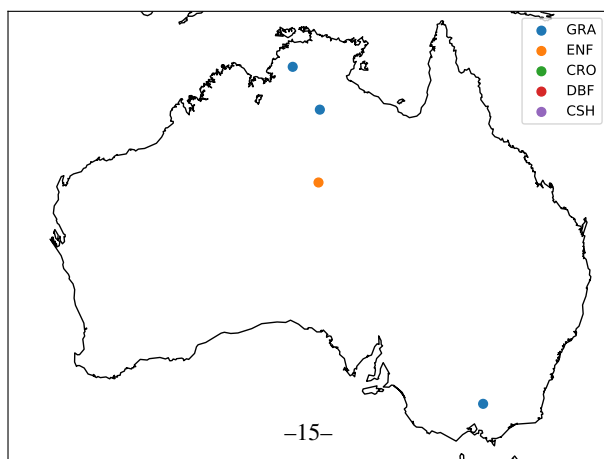
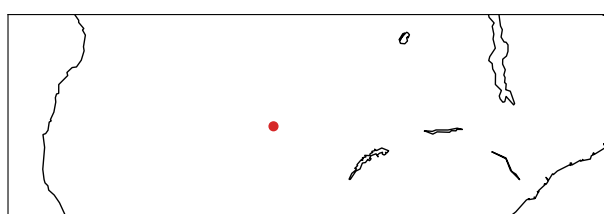
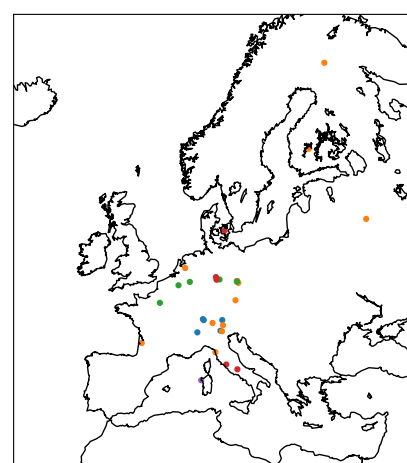
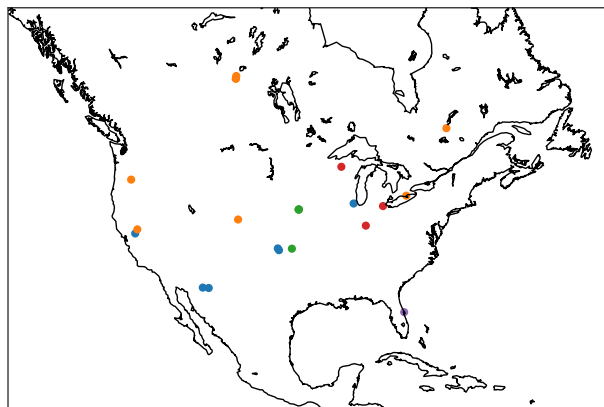
MEDLYN, B. E., R. A. DUURSMA, D. EAMUS, D. S. ELLSWORTH, I. C. PRENTICE, C. V. M. BARTON, K. Y. CROUS, P. D. ANGELIS, M. FREEMAN, and L. WINGATE (2011), Reconciling the optimal and empirical approaches to modelling stomatal conductance, *Global Change Biology*, 17(6), 2134–2144, doi:10.1111/j.1365-2486.2010.02375.x.

Zhou, S., B. Yu, Y. Huang, and G. Wang (2015), Daily underlying water use efficiency for AmeriFlux sites, *Journal of Geophysical Research: Biogeosciences*, 120(5), 887–902, doi: 10.1002/2015jg002947.

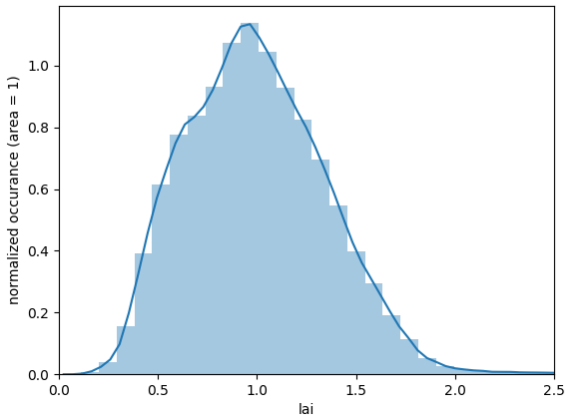
References

- (2002), A review of twentieth-century drought indices used in the united states, *Bulletin of the American Meteorological Society*, 83(8), 1149–1165, doi:10.1175/1520-0477(2002)083<1149:arotdi>2.3.co;2.
- Alley, W. M. (1984), The palmer drought severity index: Limitations and assumptions, *Journal of Climate and Applied Meteorology*, 23(7), 1100–1109, doi:10.1175/1520-0450(1984)023<1100:tpdsil>2.0.co;2.
- Ball, J. T., I. E. Woodrow, and J. A. Berry (1987), A model predicting stomatal conductance and its contribution to the control of photosynthesis under different environmental conditions, in *Progress in Photosynthesis Research*, pp. 221–224, Springer Netherlands, doi: 10.1007/978-94-017-0519-6_48.
- Franks, P. J., J. A. Berry, D. L. Lombardozzi, and G. B. Bonan (2017), Stomatal function across temporal and spatial scales: Deep-time trends, land-atmosphere coupling and global models, *Plant Physiology*, 174(2), 583–602, doi:10.1104/pp.17.00287.
- Leuning, R. (1990), Modelling stomatal behaviour and and photosynthesis ofEucalyptus grandis, *Australian Journal of Plant Physiology*, 17(2), 159, doi:10.1071/pp9900159.
- Lin, Y.-S., B. E. Medlyn, R. A. Duursma, I. C. Prentice, H. Wang, S. Baig, D. Eamus, V. R. de Dios, P. Mitchell, D. S. Ellsworth, M. O. de Beeck, G. Wallin, J. Uddling, L. Tarvainen,

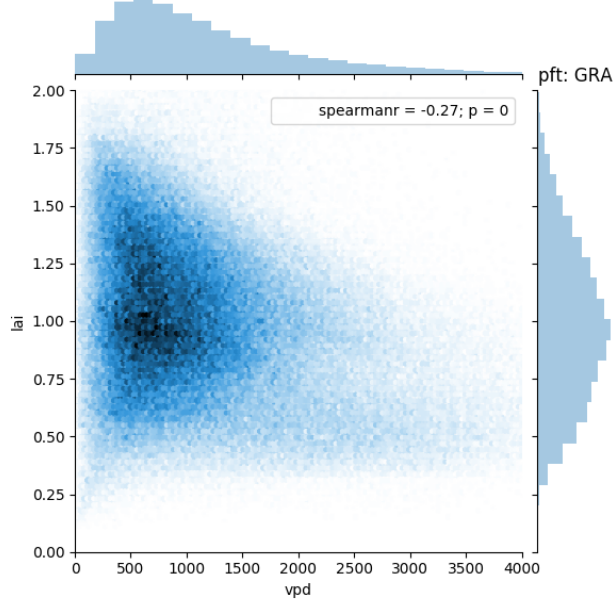
356 M.-L. Linderson, L. A. Cernusak, J. B. Nippert, T. W. Ocheltree, D. T. Tissue, N. K.
357 Martin-StPaul, A. Rogers, J. M. Warren, P. D. Angelis, K. Hikosaka, Q. Han, Y. Onoda,
358 T. E. Gimeno, C. V. M. Barton, J. Bennie, D. Bonal, A. Bosc, M. LÃºw, C. Macinins-
359 Ng, A. Rey, L. Rowland, S. A. Setterfield, S. Tausz-Posch, J. Zaragoza-Castells, M. S. J.
360 Broadmeadow, J. E. Drake, M. Freeman, O. Ghannoum, L. B. Hutley, J. W. Kelly,
361 K. Kikuzawa, P. Kolari, K. Koyama, J.-M. Limousin, P. Meir, A. C. L. da Costa, T. N.
362 Mikkelsen, N. Salinas, W. Sun, and L. Wingate (2015), Optimal stomatal behaviour
363 around the world, *Nature Climate Change*, 5(5), 459–464, doi:10.1038/nclimate2550.
364 MEDLYN, B. E., R. A. DUURSMA, D. EAMUS, D. S. ELLSWORTH, I. C. PRENTICE,
365 C. V. M. BARTON, K. Y. CROUS, P. D. ANGELIS, M. FREEMAN, and L. WINGATE
366 (2011), Reconciling the optimal and empirical approaches to modelling stomatal conduc-
367 tance, *Global Change Biology*, 17(6), 2134–2144, doi:10.1111/j.1365-2486.2010.02375.x.
368 Zhou, S., B. Yu, Y. Huang, and G. Wang (2015), Daily underlying water use efficiency for
369 AmeriFlux sites, *Journal of Geophysical Research: Biogeosciences*, 120(5), 887–902, doi:
370 10.1002/2015jg002947.



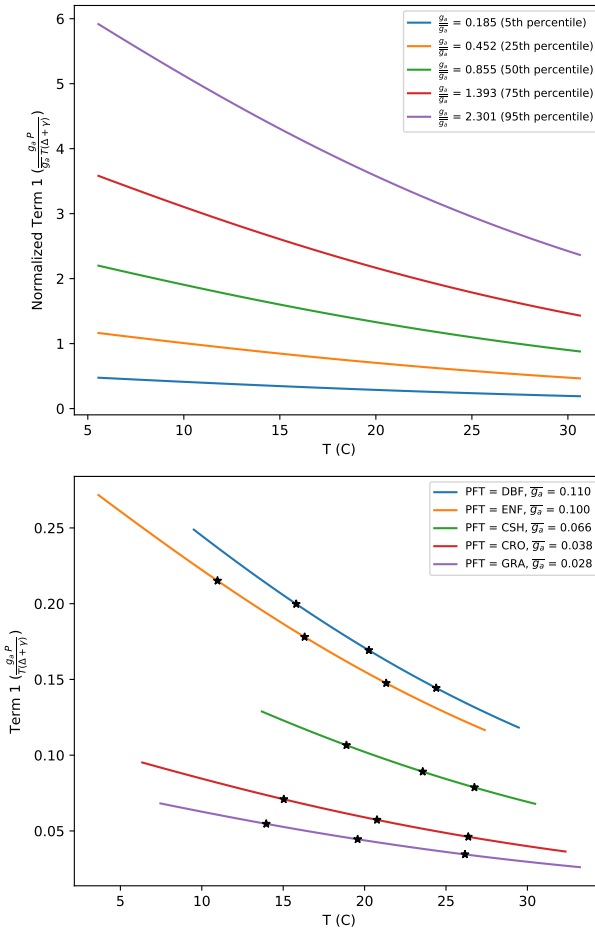
107 **Figure 1.** Plant functional type and location of sites used in analysis. ***This is just a placeholder for now
108 and needs to be improved i.e. with lat lon, better placement of continents, etc.)***



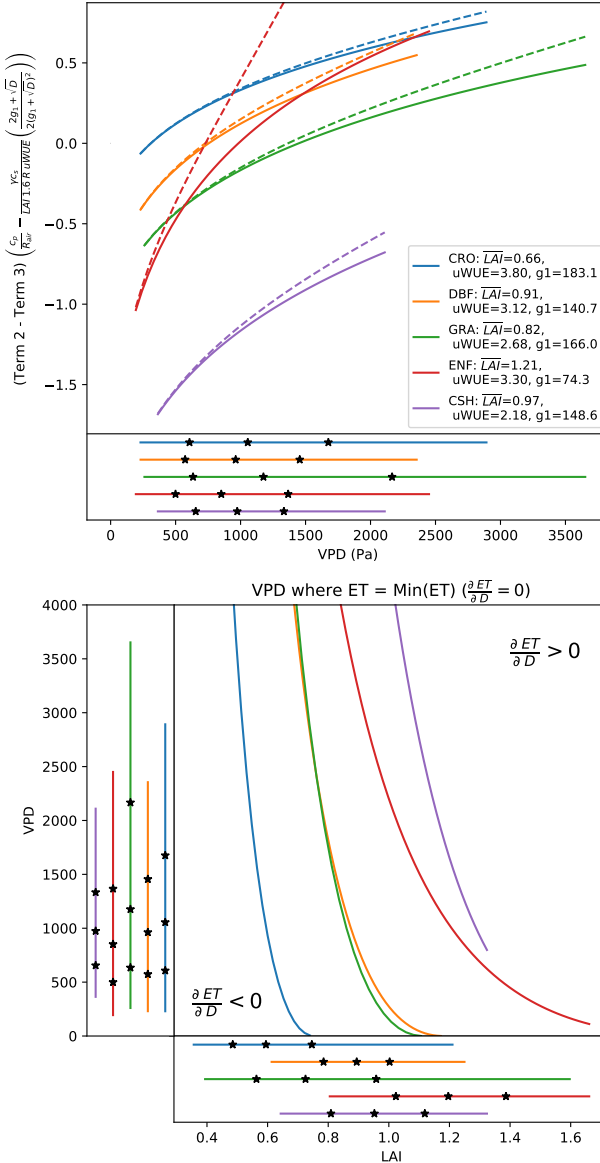
120 **Figure 2.** Histogram of σ values calculated for each site and time according to Equation 9.
 121 The lowest and highest 5% are removed as outliers, as well as any values below 0.
 122 The curve is normalized such that its area is 1.



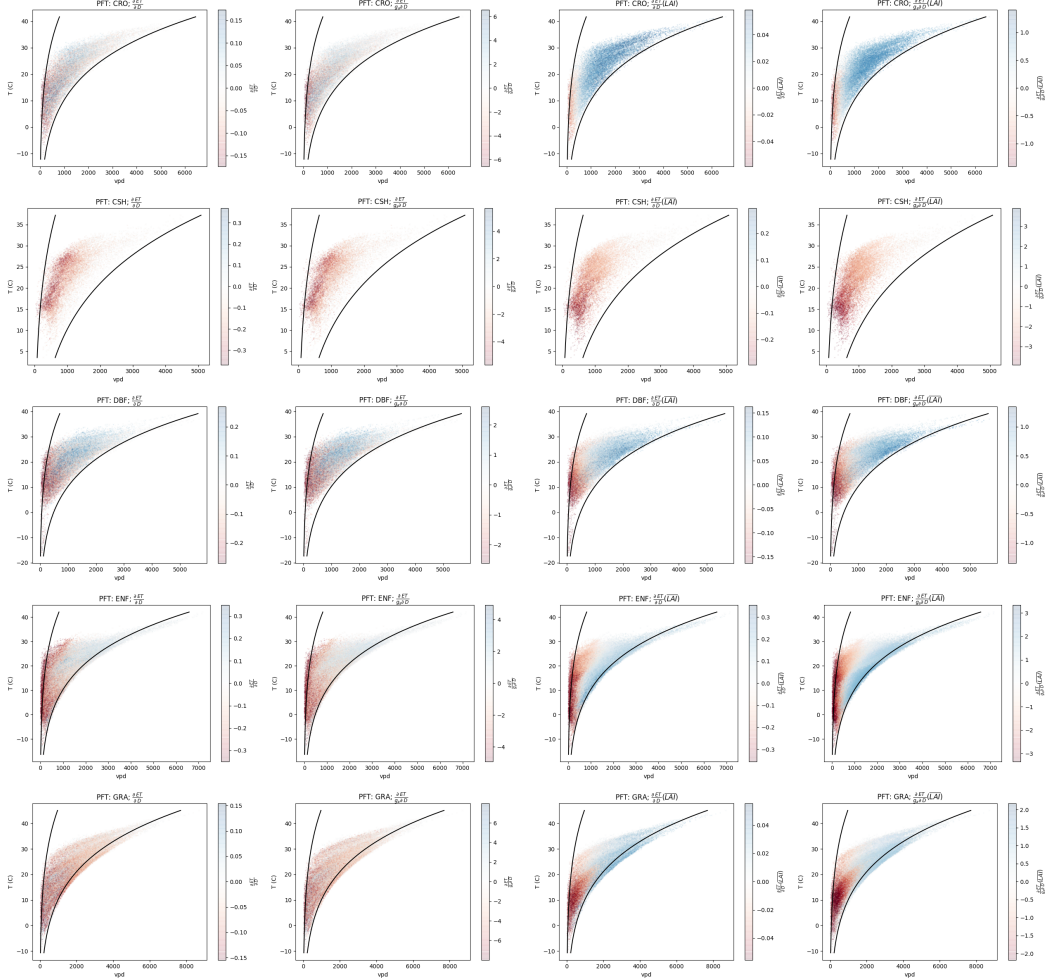
128 **Figure 3.** The joint distribution of D and σ . σ has only a weak dependence on D . ***This plot could
 129 probably benefit from a box plot of site specific correlations, because some sites do have stronger depen-
 130 dence than others. Note also Figs 3 and 2 can probably be combined because this figure shows σ 's his-
 131 togram.***



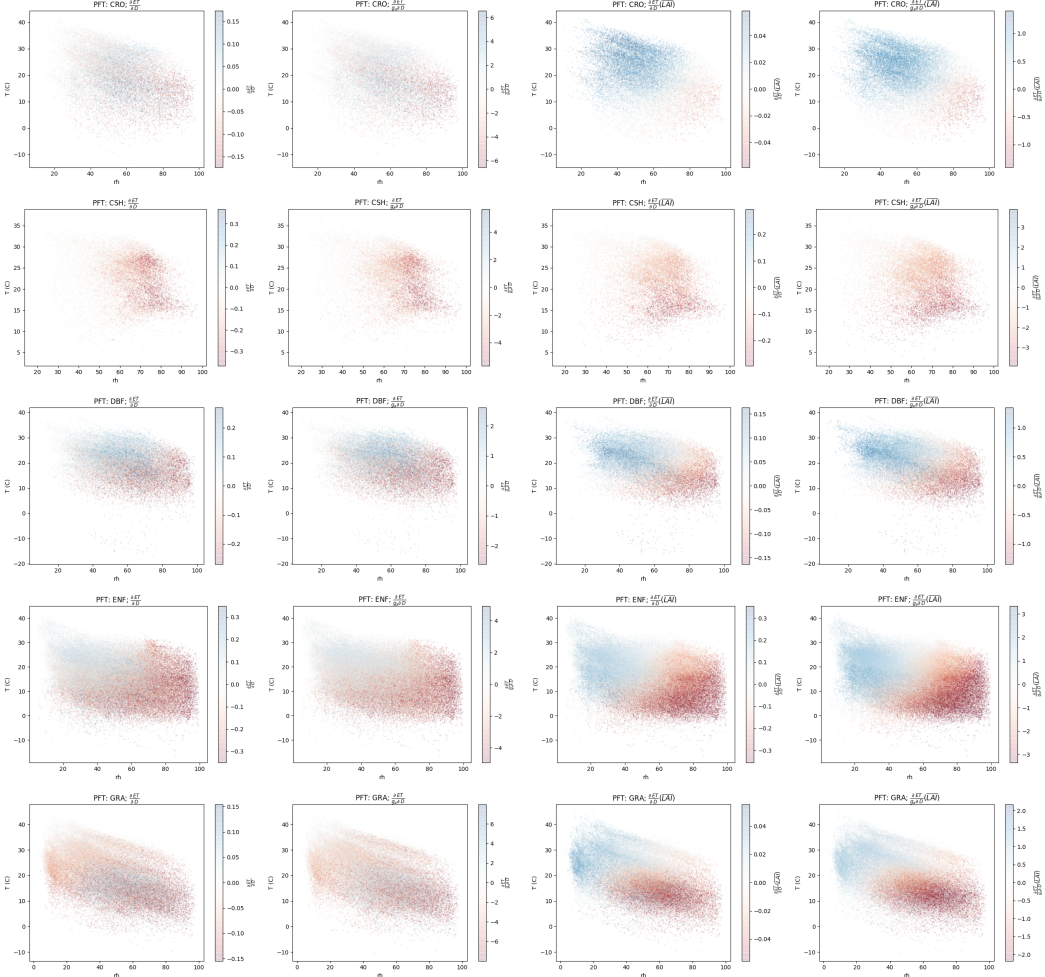
172 **Figure 4.** Primary sources of variability for Term 1. A) Variability within each PFT: Term 1 normalized by
 173 mean g_a for each PFT. B) Variability between each PFT: Term 1 evaluated at mean g_a for each PFT. Tempera-
 174 ture range is 5-95th percentile for each PFT. Additionally, stars denote the location of the 25th, 50th, and 75th
 175 percentiles.



191 **Figure 5.** Sources of variability for Term 2 - Term 3. Top: Term 2 - Term 3 as a function of VPD, with σ
 192 held fixed at PFT averages. The observed range of VPD for each PFT is also shown below the x-axis. Line
 193 extent corresponds to 5th and 95th percentiles, while stars denote the location of the 25th, 50th, and 75th
 194 percentiles.
 195 Bottom: The location of the minima of ET, as a function of VPD and σ . Lines and stars denote the distribution
 196 of VPD and σ next to each axis, following the same percentiles as above.



251 **Figure 6.** Scatter plots of $\frac{\partial ET}{\partial D}$. Each row is a different PFT, and each column is a different quantity related
 252 to $\frac{\partial ET}{\partial D}$, as labeled: Column 1 - $\frac{\partial ET}{\partial D}$; Column 2 - $\frac{\partial ET}{\partial D}$ normalized by g_a ; Column 3 - $\frac{\partial ET}{\partial D}$ with σ held
 253 fixed at PFT average; and Column 4 - $\frac{\partial ET}{\partial D}$ normalized by g_a and with σ held fixed. For reference, lines
 254 corresponding to RH = 20% and RH = 90 % are drawn. Please note differences in the colorbar scale. ***see
 255 alternate (or additional) plot below.***



263 **Figure 7.** ****alternate Fig 06**** Scatter plots of $\frac{\partial ET}{\partial D}$. Each row is a different PFT, and each column
 264 is a different quantity related to $\frac{\partial ET}{\partial D}$, as labeled. If I end up using this, I could also draw on the curve of
 265 D_{ETmin} with $\overline{\text{LAI}_{ref}}$.